Published in final edited form as:

Mol Pharm. 2019 October 07; 16(10): 4416–4421. doi:10.1021/acs.molpharmaceut.9b00746.

Dual Radionuclide Theranostic Pretargeting

Outi Keinänen[1], **James Brennan**[1], **Rosemery Membreno**[1,2,†], **Kimberly Fung**[1,2], **Kishore Gangangari**[1,2,§], **Eric Dayts**[1], **Carter J. Williams**[1], **Brian M. Zeglis**[1,2,3,4,*]

[1]Department of Chemistry, Hunter College, City University of New York, New York, NY, USA, 10021

[2]Ph.D. Program in Chemistry, The Graduate Center of the City University of New York, New York, NY, USA, 10016

[3]Department of Radiology, Memorial Sloan Kettering Cancer Center, New York, NY, USA, 10065

[4]Department of Radiology, Weill Cornell Medical College, New York, NY, USA, 10065

Abstract

Recent years have played witness to the advent of nuclear theranostics: the synergistic use of 'matched pair' radiopharmaceuticals for diagnostic imaging and targeted radiotherapy. In this investigation, we report the extension of this concept to *in vivo* pretargeting based on the rapid and bioorthogonal inverse electron demand Diels-Alder reaction between tetrazine (Tz) and *trans*-cyclooctene (TCO). We demonstrate that a single injection of a TCO-modified immunoconjugate can be used as a platform for pretargeted PET imaging and radiotherapy via the sequential administration of a pair of Tz-bearing radioligands labeled with the positron-emitting radiometal copper-64 ($t_{1/2}$ ~ 12.7 h) and the beta-emitting radiometal lutetium-177 ($t_{1/2}$ ~ 6.7 d). More specifically, a mouse model of human colorectal carcinoma received a dose of the A33 antigen-targeting immunoconjugate huA33-TCO, followed 24 and 48 h later by injections of [^{64}Cu]Cu-SarAr-Tz and [^{177}Lu]Lu-DOTA-PEG$_7$-Tz, respectively. This approach produces high activity concentrations of both radioligands in tumor tissue (16.4 ± 2.7 %ID/g for [^{64}Cu]Cu-SarAr-Tz at 48 h post-injection and 18.1 ± 2.1 %ID/g for [^{177}Lu]Lu-DOTA-PEG$_7$-Tz at 120 h post-injection) as well as promising tumor-to-healthy organ activity concentration ratios. Ultimately, we believe that this work could not only have important implications in nuclear theranostics — most excitingly with isotopologue-based radioligand pairs such as [^{64}Cu]Cu-SarAr-Tz and [^{67}Cu]Cu-SarAr-Tz — but also in the delivery of fractionated doses during pretargeted radioimmunotherapy.

*Corresponding Author: Brian M. Zeglis. 413 East 69th Street, New York, NY, 10021. Phone: 212-896-0433. Fax: 212-772-5332. bz102@hunter.cuny.edu.

†**Present Address** Rosemery Membreno: World Molecular Imaging Society, Culver City, CA, 90230, USA

§**Present Address** Kishore Gangangari: Charles River Associates, New York, NY 10018, USA

Author Contributions

The manuscript was written through contributions of all authors. All authors have given approval to the final version of the manuscript.

All animals were treated according to the guidelines approved by the Research Animal Resource Center and Institutional Animal Care and Use Committee at Memorial Sloan Kettering Cancer Center. The authors declare no competing financial interest.

ASSOCIATED CONTENT

Supporting Information

The Supporting Information is available free of charge on the ACS Publications website at DOI: 10.1021/acs.molpharmaceut.xxxxxx. Reagents and general procedures; detailed experimental methods for chemical syntheses, radiosyntheses, and *in vivo* experiments; PET imaging protocols; dosimetry calculations; tables of biodistribution data, both activity concentrations and tumor-to-tissue activity concentration ratios; calculation of the fraction of TCO moieties available to react with the second radioligand.

Graphical Abstract

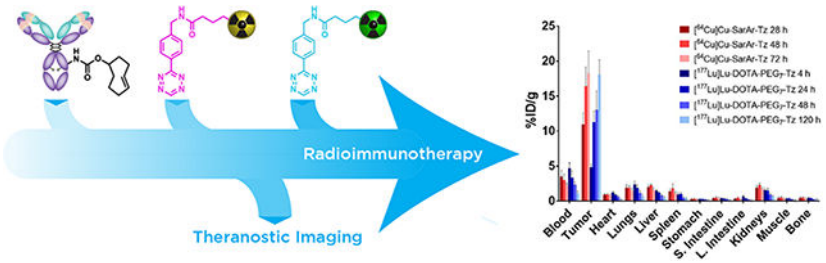

Keywords

Pretargeting; multistep targeting; inverse electron demand Diels-Alder reaction; tetrazine; *trans*-cyclooctene; click chemistry; bioorthogonal chemistry; positron emission tomography; PET; theranostics; pretargeted radioimmunotherapy; colorectal cancer; huA33; A33 antigen

Introduction

Over the past decade, the concept of ‘nuclear theranostics’ has emerged as a critical clinical tool.[1,2] Broadly defined, nuclear theranostics describes the synergistic use of ‘matched pair’ radiopharmaceuticals for diagnostic imaging and targeted endoradiotherapy. Indeed, the use of companion nuclear imaging agents based on the same platform as targeted radiotherapeutics facilitates the selection of patients most likely to respond to treatment, enables the optimization of the dose of the radiotherapeutic, and allows for the longitudinal monitoring of patients during treatment. As a result, the advent of theranostics clearly offers a path to more personalized and precise care. This paradigm has been leveraged with great success in the clinic. For example, [^{68}Ga]Ga-DOTA-TATE has been effectively employed for the diagnostic PET imaging of patients with neuroendocrine tumors receiving peptide receptor radiotherapy with [^{177}Lu]Lu-DOTA-TATE.[3,4] Likewise, [^{68}Ga]Ga-PSMA-617 has shown promise for the PET imaging of prostate cancer patients undergoing treatment with [^{177}Lu]Lu-PSMA-617 or [^{225}Ac]Ac-PSMA-617.[5–8] This approach is not limited to ^{68}Ga-labeled PET imaging agents, of course: several ^{89}Zr-labeled antibodies have also been used as companion imaging agents for radioimmunotherapeutics labeled with nuclides including yttrium-90, lutetium-177, and actinium-225.

In the investigation at hand, our goal was to develop a theranostic approach to *in vivo* pretargeting. While radioimmunotherapy has long shown promise as a treatment strategy, the prolonged circulation times of radioimmunoconjugates — and, consequently, their high radiation doses to healthy tissues — has hampered their clinical utility. One way to circumvent this limitation is *in vivo* pretargeting. Pretargeting, in essence, relies upon performing radiosynthesis *within* the body. The antibody is injected prior to the radionuclide, and the two components are designed to combine at the tumor itself. In this way, this approach effectively delivers radioactivity to target tissues while shortening the circulation time of the radioactivity and facilitating the use of short-lived nuclides (*e.g.* copper-64, fluorine-18, and gallium-68) that are normally incompatible with vectors with long pharmacokinetic half-lives.

Over the last half decade — in conjunction with our collaborators and in parallel with a handful of other laboratories — we have developed an approach to *in vivo* pretargeting based on the rapid and bioorthogonal inverse electron demand Diels-Alder (IEDDA) ligation between a *trans*-cyclooctene (TCO)-modified antibody and a tetrazine (Tz)-bearing radioligand (Figure 1A).[9–14] This methodology has five elemental steps: (i) the administration of the TCO-bearing immunoconjugate; (ii) an interval period during which the mAb-TCO slowly accumulates in the target tissue and clears from the blood; (iii) the administration of the small molecule Tz radioligand; (iv) the *in vivo* click ligation between the two components; and (v) the rapid clearance of any excess radioligand. In murine models of pancreatic, colorectal, and breast cancer, we have demonstrated that this approach can be effectively harnessed for PET imaging with ^{64}Cu ($t_{1/2}$ ~ 12.7 h), ^{18}F ($t_{1/2}$ ~ 110 min), and ^{68}Ga ($t_{1/2}$ ~ 68 min).[15–20] Just as — and perhaps even more — importantly, we have also used mouse models of pancreatic and colorectal cancer to illustrate the efficacy of IEDDA-based pretargeted radioimmunotherapy (PRIT) with both ^{177}Lu ($t_{1/2}$ ~ 6.7 d) and ^{225}Ac ($t_{1/2}$ ~ 10.0 d).[21–23] In both applications, this *in vivo* pretargeting strategy produces high activity concentrations in tumor tissue. Furthermore, the radiation dose rates to healthy tissues created by this methodology — particularly in the context of pretargeted PET with ^{68}Ga or ^{18}F — are far lower than those created by traditional radioimmunoconjugates labeled with long-lived radionuclides such as zirconium-89 ($t_{1/2}$ ~ 3.3 d) or iodine-124 ($t_{1/2}$ ~ 4.2 d). As IEDDA-based PRIT continues its steady progression toward the clinic, it is likely that it will ultimately benefit from a theranostic approach, just as endoradiotherapy with [^{177}Lu]Lu-DOTA-TATE, [^{177}Lu]Lu-PSMA-617, and radioimmunoconjugates have

Results

Our theranostic pretargeting strategy is predicated on following the injection of the mAb-TCO with the sequential administration of not one but *two* radioligands: one for PET and one for endoradiotherapy (Figure 2A). Critically, the PET imaging of the former could provide information on the biodistribution, and thus dosimetry, of the latter. The feasibility of this approach, however, requires that the *trans*-cyclooctene moieties of the TCO-bearing immunoconjugate are not fully saturated after the initial injection of a Tz-based radioligand and thus can subsequently react with a second radioligand. Fortunately, this seems to be the case. Based on previous biodistribution experiments and several inevitable (yet, we argue, reasonable) assumptions, we estimate that the injection of the initial radioligand occupies about ~15% of the antibody-bound TCO moieties and that 0.32 nmol of the TCO groups have isomerized to *cis*-cyclooctene (CCO) 48 h after the administration of huA33-TCO. Taken together, these two processes leave ~64% of the injected TCOs free to react with a second radioligand (see Supporting Information for calculation). The two radioligands we have used in this investigation — [^{64}Cu]Cu-SarAr-Tz and [^{177}Lu]Lu-DOTA-PEG$_7$-Tz — have already proven highly effective for pretargeted PET imaging and radioimmunotherapy, respectively (Figure 1B).[13, 24] Admittedly, the use of two structurally different radioligands falls somewhat short of the theranostic matched pair ideal represented by [^{68}Ga]Ga-PSMA-617 and [^{177}Lu]Lu-PSMA-617 or, even more stringently, isotopologue-based radiopharmaceuticals. However, [^{64}Cu]Cu-SarAr-Tz and [^{177}Lu]Lu-DOTA-PEG$_7$-Tz boast very similar pharmacokinetic profiles, serum half-lives, and reaction kinetics with *trans*-

cyclooctene, making the pair a suitable choice for this proof-of-concept investigation (Supporting Information Tables S1 and S2).[13, 21, 22, 24] Finally, our model system is rounded out by the huA33 antibody 3/4 an IgG that targets a transmembrane glycoprotein (the A33 antigen) expressed by >95% of colorectal carcinomas 3/4 and the A33 antigen-expressing SW1222 human colorectal cancer cell line.[25–27]

For the investigation at hand, huA33-TCO, [^{64}Cu]Cu-SarAr-Tz, and [^{177}Lu]Lu-DOTA-PEG$_7$-Tz were synthesized, purified, and characterized according to previously published procedures.[13, 15, 17, 21] Female athymic nude mice (5–7 weeks old) were inoculated with 5×10^6 SW1222 cells in the right shoulder, and the subcutaneous xenografts were allowed to grow for two weeks. Once the tumors had grown to an appropriate size (~100 mm^3), huA33-TCO (100 μg, 0.67 nmol, 2.4 TCO/mAb) was administered intravenously (*i.v.*) via the tail vein. The first radioligand — [^{64}Cu]Cu-SarAr-Tz (10.4–11.3 MBq, 0.64–0.70 nmol) — was then administered 24 h later, followed 24 h thereafter by the second radioligand, [^{177}Lu]Lu-DOTA-PEG$_7$-Tz (5.9–6.4 MBq, 0.69–0.74 nmol) (Figure 2B). PET imaging was then carried out 6, 24, and 48 h after the administration of [^{64}Cu]Cu-SarAr-Tz. In a parallel biodistribution experiment, mice were sacrificed 4, 24, 48, and 120 h after the injection of [^{177}Lu]Lu-DOTA-PEG$_7$-Tz, and their organs were collected, weighed, and measured for both ^{64}Cu and ^{177}Lu using a gamma counter. The *i.v.* injections of the two radioligands were performed using opposite tail veins. This 24 h interval between the administration of the two radiotracers was chosen for three reasons: (*i*) it provides more than enough time for any unreacted [^{64}Cu]Cu-SarAr-Tz to clear from the blood prior to the administration of [^{177}Lu]Lu-DOTA-PEG$_7$-Tz (Supporting Information Table S1); (*ii*) it facilitates the collection of several high quality PET scans before the injection of the ^{177}Lu-labeled radioligand; and (*iii*) it allows for a significant amount of time during which both types of radioactivity are present in the body, enabling comparisons between the biodistribution profiles of both radioligands.

The PET images and biodistribution results produced by [^{64}Cu]Cu-SarAr-Tz (Figure 3B and Table 1) closely mirror our previous work with this system (Supporting Information Tables S3 and S4).[13, 16, 20] Tumoral uptake of the ^{64}Cu-labeled tetrazine is evident at early time points and increases to a maximum of 18.3 ± 3.1 %ID/g at 72 h post-injection. Some activity is present in the blood at early time points (3.5 ± 0.9 %ID/g at 28 h p.i.), likely the result of click reactions between [^{64}Cu]Cu-SarAr-Tz and still circulating huA33-TCO. However, these activity concentrations decrease with time, ultimately yielding a tumor-to-blood activity concentration ratio of 8.2 ± 1.6 at 72 h post-injection (Supporting Information Table S5). Other healthy organs generally exhibit very low activity concentrations: to wit, the non-target tissues with the *highest* uptake — the liver and the kidneys — contain <2% ID/g at 72 h p.i. The more notable biodistribution results are provided by the second radioligand: [^{177}Lu]Lu-DOTA-PEG$_7$-Tz. Surprisingly, the prior administration of [^{64}Cu]Cu-SarAr-Tz does not appear to dramatically hinder the *in vivo* performance of the ^{177}Lu-labeled tetrazine (Table 1 and Supporting Information Table S4). The tumoral activity concentration is 4.9 ± 0.4 %ID/g at 4 h p.i., a value which increases to 13.1 ± 2.7 %ID/g and 18.1 ± 2.1 %ID/g at 48 and 120 h post-injection, respectively. As in the ^{64}Cu case, activity can be observed in the blood at early time points, but this decreases with time to ultimately produce a tumor-to-blood activity concentration ratio of 17.9 ± 5.9 at 120 h post-injection (Supporting

Information Table S5). Furthermore, the activity concentrations in healthy organs are also all quite low, generally under 1–2 %ID/g. Analogous theranostic pretargeting experiments with a 6 h — rather than 24 h — interval between the administration of [^{64}Cu]Cu-SarAr-Tz and [^{177}Lu]Lu-DOTA-PEG$_7$-Tz produced strikingly similar results, illustrating that this phenomenon is not the product of a single set of reaction conditions (Supporting Information Figure S1 and Tables S6 and S7).

Discussion

Taken together, these *in vivo* data prompt two important observations. First, the biodistribution profile of the pretargeted [^{64}Cu]Cu-SarAr-Tz is very similar to that of [^{177}Lu]Lu-DOTA-PEG$_7$-Tz, suggesting that the former could be used as a companion imaging agent for the latter. Indeed, at 48 h post-injection, for example, the correlation between the uptake of the two radioligands in different tissues is remarkably high. Second, as we have noted, the previous administration of [^{64}Cu]Cu-SarAr-Tz does not appear to have significant adverse effects on the biodistribution of [^{177}Lu]Lu-DOTA-PEG$_7$-Tz. In an earlier study by Membreno *et al.*[21] in which [^{177}Lu]Lu-DOTA-PEG$_7$-Tz was injected 48 h after the administration of huA33 — but *without* the intervening injection of [^{64}Cu]Cu-SarAr-Tz — the tumoral activity concentrations at 48 and 120 h post-injection were 13.0 ± 2.8 and 11.0 ± 2.4 %ID/g, similar to the 13.1 ± 2.7 and 18.1 ± 2.1 %ID/g value obtained in this experiment (Supporting Information Table S3). Critically, the activity concentrations in other non-target organs were similar across the two investigations as well.

In order to further explore the potential of this approach for PRIT, dosimetry calculations were performed based on the [^{177}Lu]Lu-DOTA-PEG$_7$-Tz biodistribution data (Table 2). For most tissues, the time-activity curves could be best fit using one- or two-phase exponential decay models. Yet for the tumor — which displayed increased uptake over the experiment — a trapezoidal model was used up until the last time point, after which it was assumed that clearance was based entirely on radioactive decay. The dosimetry calculations revealed a total absorbed dose to the tumor of 310.2 cGy/MBq and a tumor-to-blood therapeutic index of 12.4. These results are consistent with (though slightly lower than) those obtained by Membreno, *et al.* in their proof-of-concept study of colorectal cancer PRIT with huA33-TCO and [^{177}Lu]Lu-DOTA-PEG$_7$-Tz (Supporting Information Table S8).[21] This strongly suggests that this theranostic pretargeting approach could likewise be used for effective radiotherapy in mice bearing SW1222 xenografts.

Herein, we have described the development of a proof-of-concept system for theranostic pretargeting based on a single immunoconjugate (huA33-TCO) and a pair of radioligands labeled with diagnostic ([^{64}Cu]Cu-SarAr-Tz) and therapeutic ([^{177}Lu]Lu-DOTA-PEG$_7$-Tz) radionuclides. We believe that this system could be used to help select patients for PRIT and optimize the dose and timing of PRIT regimens. Yet our observations regarding the sequential administration of the tetrazine-based radioligands could be just as important as the theranostic implications of this work. Our data clearly indicate that the administration of a second Tz-bearing radioligand is feasible in the context of IEDDA-based pretargeting. And even more importantly, the *in vivo* performance of the second radioligand seems to be largely unaffected by the administration of the first. We believe that this phenomenon could

have a significant impact not only on theranostic pretargeting but also on the administration of fractionated doses during PRIT. Moving forward, we plan to leverage this work in three ways: exploring theranostic pretargeting with longer injection intervals (*e.g.* 72 h between the administration of the two radioligands), developing new theranostic pretargeting systems based on chemically identical isotopologue-containing radioligands (*e.g.* ^{67}Cu/^{64}Cu), and examining the benefits of fractionated dosing in the context of PRIT with ^{67}Cu, ^{177}Lu-, and ^{225}Ac-labeled radioligands.

Supplementary Material

Refer to Web version on PubMed Central for supplementary material.

Acknowledgment

Dr. Lukas Carter is gratefully acknowledged for the help with dosimetry calculations and PET image reconstruction.

Funding Sources

National Institutes of Health (R01CA204167, U01CA221046, and R01CA240963). Services provided by the MSKCC Small-Animal Imaging Core Facility were supported in part by NIH grants R24 CA83084 and P30 CA08748.

Abbreviations

%ID/g	percent injected dose per gram
IEDDA	inverse electron demand Diels-Alder
iTLC	instant thin layer chromatography
PET	positron emission tomography
p.i.	post-injection
PRIT	pretargeted radioimmunotherapy
RIT	radioimmunotherapy
TCO	*trans*-cyclooctene
Tz	tetrazine

REFERENCES

1. Eberlein U; Cremonesi M; Lassmann M Individualized dosimetry for theranostics: Necessary, nice to have, or counterproductive? Journal of Nuclear Medicine 2017, 58, (Supplement 2), 97S–103S. [PubMed: 28864620]
2. Turner JH An introduction to the clinical practice of theranostics in oncology. The British Journal of Radiology 2018, 91, (1091), 20180440. [PubMed: 30179054]
3. Kjaer A; Knigge U Use of radioactive substances in diagnosis and treatment of neuroendocrine tumors. Scandinavian Journal of Gastroenterology 2015, 50, (6), 740–7. [PubMed: 25959100]

4. Schottelius M; Simecek J; Hoffmann F; Willibald M; Schwaiger M; Wester HJ Twins in spirit - episode I: comparative preclinical evaluation of [68Ga]DOTATATE and [68Ga]HA-DOTATATE. EJNMMI Research 2015, 5, 22. [PubMed: 25918675]
5. Benesova M; Schafer M; Bauder-Wust U; Afshar-Oromieh A; Kratochwil C; Mier W; Haberkorn U; Kopka K; Eder M Preclinical evaluation of a tailor-made DOTA-conjugated PSMA inhibitor with optimized linker moiety for imaging and endoradiotherapy of prostate cancer. Journal of Nuclear Medicine 2015, 56, (6), 914–20. [PubMed: 25883127]
6. Afshar-Oromieh A; Hetzheim H; Kratochwil C; Benesova M; Eder M; Neels OC; Eisenhut M; Kubler W; Holland-Letz T; Giesel FL; Mier W; Kopka K; Haberkorn U The theranostic PSMA ligand PSMA-617 in the diagnosis of prostate cancer by PET/CT: Biodistribution in humans, radiation dosimetry, and first evaluation of tumor lesions. Journal of Nuclear Medicine 2015, 56, (11), 1697–705. [PubMed: 26294298]
7. Kratochwil C; Bruchertseifer F; Giesel FL; Weis M; Verburg FA; Mottaghy F; Kopka K; Apostolidis C; Haberkorn U; Morgenstern A ^{225}Ac-PSMA-617 for PSMA-targeted α-radiation therapy of metastatic castration-resistant prostate cancer. Journal of Nuclear Medicine 2016, 57, (12), 1941–1944. [PubMed: 27390158]
8. Ballinger JR Theranostic radiopharmaceuticals: established agents in current use. British Journal of Radiology 2018, 91, (1091), 20170969. [PubMed: 29474096]
9. Rossin R; Verkerk PR; van den Bosch SM; Vulders RC; Verel I; Lub J; Robillard MS In vivo chemistry for pretargeted tumor imaging in live mice. Angewandte Chemie International Edition 2010, 49, (19), 3375–8. [PubMed: 20391522]
10. Rossin R; van den Bosch SM; Ten Hoeve W; Carvelli M; Versteegen RM; Lub J; Robillard MS Highly reactive trans-cyclooctene tags with improved stability for Diels-Alder chemistry in living systems. Bioconjugate Chemistry 2013, 24, (7), 1210–7. [PubMed: 23725393]
11. Rossin R; van Duijnhoven SM; Lappchen T; van den Bosch SM; Robillard MS Trans-cyclooctene tag with improved properties for tumor pretargeting with the diels-alder reaction. Molecular Pharmaceutics 2014, 11, (9), 3090–6. [PubMed: 25077373]
12. Zeglis BM; Sevak KK; Reiner T; Mohindra P; Carlin SD; Zanzonico P; Weissleder R; Lewis JS A pretargeted PET imaging strategy based on bioorthogonal Diels-Alder click chemistry. Journal of Nuclear Medicine 2013, 54, (8), 1389–96. [PubMed: 23708196]
13. Zeglis BM; Brand C; Abdel-Atti D; Carnazza KE; Cook BE; Carlin S; Reiner T; Lewis JS Optimization of a pretargeted strategy for the PET imaging of colorectal carcinoma via the modulation of radioligand pharmacokinetics. Molecular Pharmaceutics 2015, 12, (10), 3575–87. [PubMed: 26287993]
14. Blackman ML; Royzen M; Fox JM Tetrazine ligation: Fast bioconjugation based on inverse-electron-demand Diels−Alder reactivity. Journal of the American Chemical Society 2008, 130, (41), 13518–13519. [PubMed: 18798613]
15. Houghton JL; Zeglis BM; Abdel-Atti D; Sawada R; Scholz WW; Lewis JS Pretargeted immuno-PET of pancreatic cancer: Overcoming circulating antigen and internalized antibody to reduce radiation doses. Journal of Nuclear Medicine 2016, 57, (3), 453–9. [PubMed: 26471693]
16. Cook BE; Adumeau P; Membreno R; Carnazza KE; Brand C; Reiner T; Agnew BJ; Lewis JS; Zeglis BM Pretargeted PET imaging using a site-specifically labeled immunoconjugate. Bioconjugate Chemistry 2016, 27, (8), 1789–1795. [PubMed: 27356886]
17. Cook BE; Membreno R; Zeglis BM Dendrimer Scaffold for the Amplification of In Vivo Pretargeting Ligations. Bioconjugate Chemistry 2018, 29, (8), 2734–2740. [PubMed: 29969558]
18. Meyer JP; Houghton JL; Kozlowski P; Abdel-Atti D; Reiner T; Pillarsetty NV; Scholz WW; Zeglis BM; Lewis JS ^{18}F-Based pretargeted PET imaging based on bioorthogonal Diels-Alder click chemistry. Bioconjugate Chemistry 2016, 27, (2), 298–301. [PubMed: 26479967]
19. Meyer JP; Kozlowski P; Jackson J; Cunanan KM; Adumeau P; Dilling TR; Zeglis BM; Lewis JS Exploring structural parameters for pretargeting radioligand optimization. Journal of Medicinal Chemistry 2017, 60, (19), 8201–8217. [PubMed: 28857566]
20. Adumeau P; Carnazza KE; Brand C; Carlin SD; Reiner T; Agnew BJ; Lewis JS; Zeglis BM A Pretargeted Approach for the Multimodal PET/NIRF Imaging of Colorectal Cancer. Theranostics 2016, 6, (12), 2267–2277. [PubMed: 27924162]

21. Membreno R; Cook BE; Fung K; Lewis JS; Zeglis BM Click-mediated pretargeted radioimmunotherapy of colorectal carcinoma. Molecular Pharmaceutics 2018, 15, (4), 1729–1734. [PubMed: 29502416]

22. Membreno R; Keinänen OM; Cook BE; Tully KM; Fung KC; Lewis JS; Zeglis BM Towards the optimization of click-mediated pretargeted radioimmunotherapy. Molecular Pharmaceutics 2019, 16, (5), 2259–2263. [PubMed: 30912951]

23. Poty S; Carter LM; Mandleywala K; Membreno R; Abdel-Atti D; Ragupathi A; Scholz WW; Zeglis BM; Lewis JS Leveraging bioorthogonal click chemistry to improve (225)Ac-radioimmunotherapy of pancreatic ductal adenocarcinoma. Clinical Cancer Research 2019, 25, (2), 868–880. [PubMed: 30352909]

24. Houghton JL; Membreno R; Abdel-Atti D; Cunanan KM; Carlin S; Scholz WW; Zanzonico PB; Lewis JS; Zeglis BM Establishment of the in vivo efficacy of pretargeted radioimmunotherapy utilizing inverse electron demand Diels-Alder click chemistry. Molecular Cancer Therapeutics 2017, 16, (1), 124–133. [PubMed: 28062708]

25. Heath JK; White SJ; Johnstone CN; Catimel B; Simpson RJ; Moritz RL; Tu GF; Ji H; Whitehead RH; Groenen LC; Scott AM; Ritter G; Cohen L; Welt S; Old LJ; Nice EC; Burgess AW The human A33 antigen is a transmembrane glycoprotein and a novel member of the immunoglobulin superfamily. Proceedings of the National Academy of Sciences of the United States of America 1997, 94, (2), 469–74. [PubMed: 9012807]

26. Welt S; Scott AM; Divgi CR; Kemeny NE; Finn RD; Daghighian F; Germain JS; Richards EC; Larson SM; Old LJ Phase I/II study of iodine 125-labeled monoclonal antibody A33 in patients with advanced colon cancer. Journal of Clinical Oncology 1996, 14, (6), 1787–97. [PubMed: 8656247]

27. Scott AM; Lee FT; Jones R; Hopkins W; MacGregor D; Cebon JS; Hannah A; Chong G; U, P.; Papenfuss A; Rigopoulos A; Sturrock S; Murphy R; Wirth V; Murone C; Smyth FE; Knight S; Welt S; Ritter G; Richards E; Nice EC; Burgess AW; Old LJ A phase I trial of humanized monoclonal antibody A33 in patients with colorectal carcinoma: biodistribution, pharmacokinetics, and quantitative tumor uptake. Clinical Cancer Research 2005, 11, (13), 4810–7. [PubMed: 16000578]

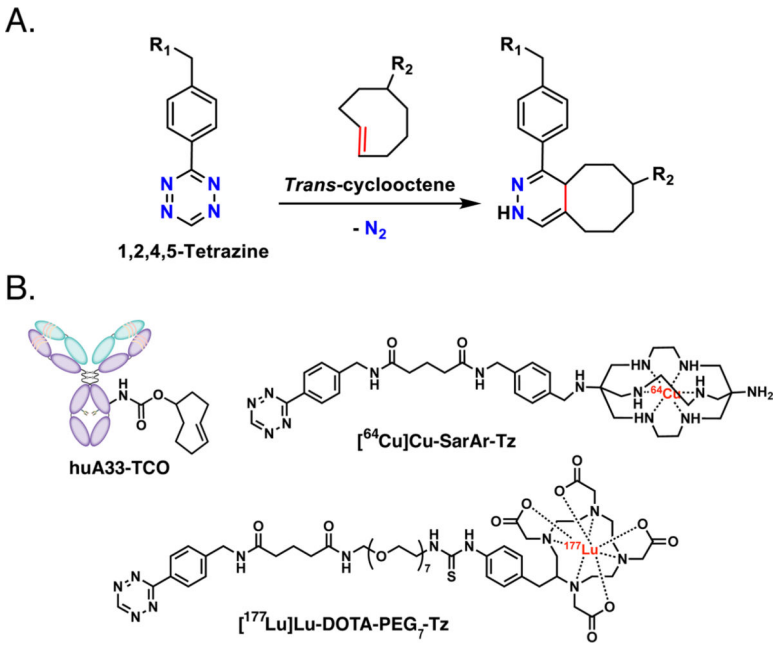

Figure 1.

(A) The inverse electron demand Diels-Alder (IEDDA) reaction between *trans*-cyclooctene and tetrazine; (B) a schematic of huA33-TCO and the structures of [^{64}Cu]Cu-SarAr-Tz and [^{177}Lu]Lu-DOTA-PEG$_7$-Tz.

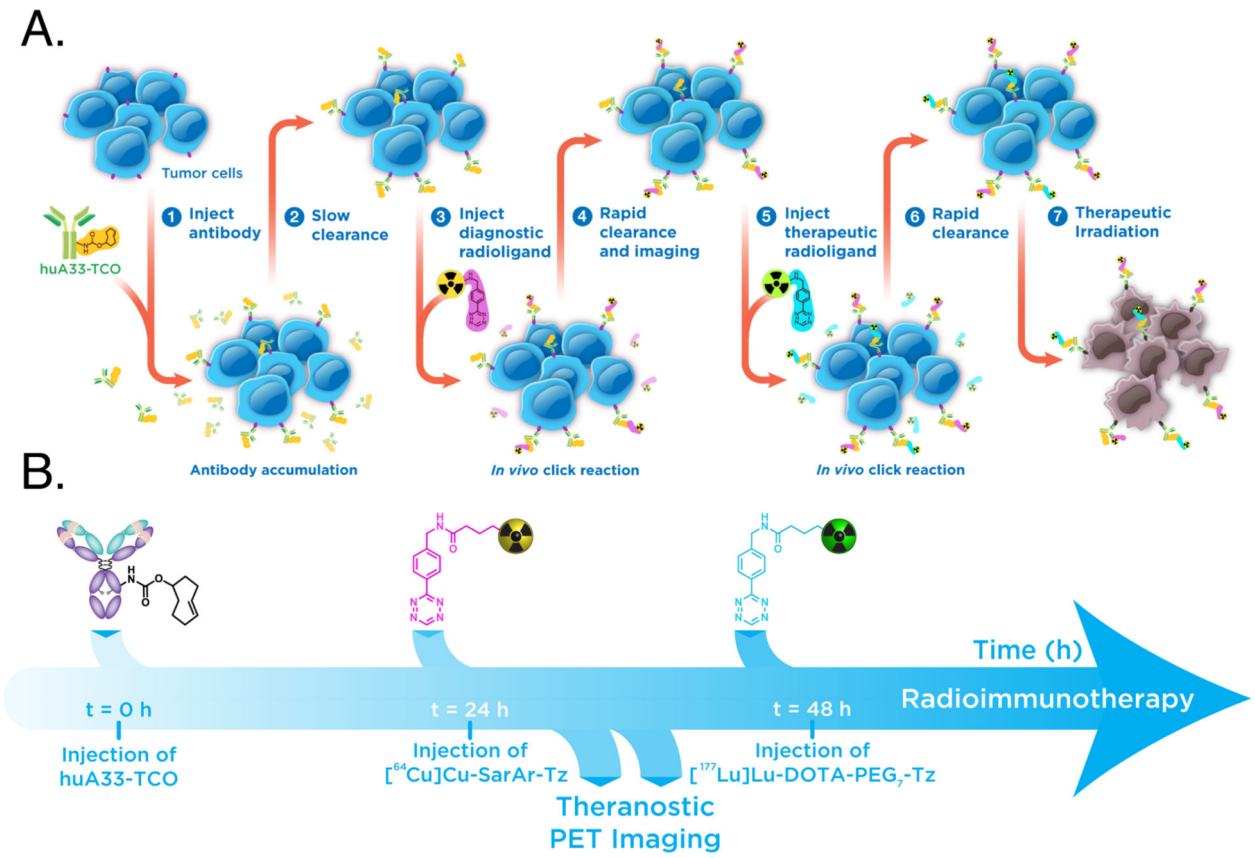

Figure 2.

(A) A schematic of dual radionuclide theranostic pretargeting based on the IEDDA reaction; (B) a timeline of the sequence of events.

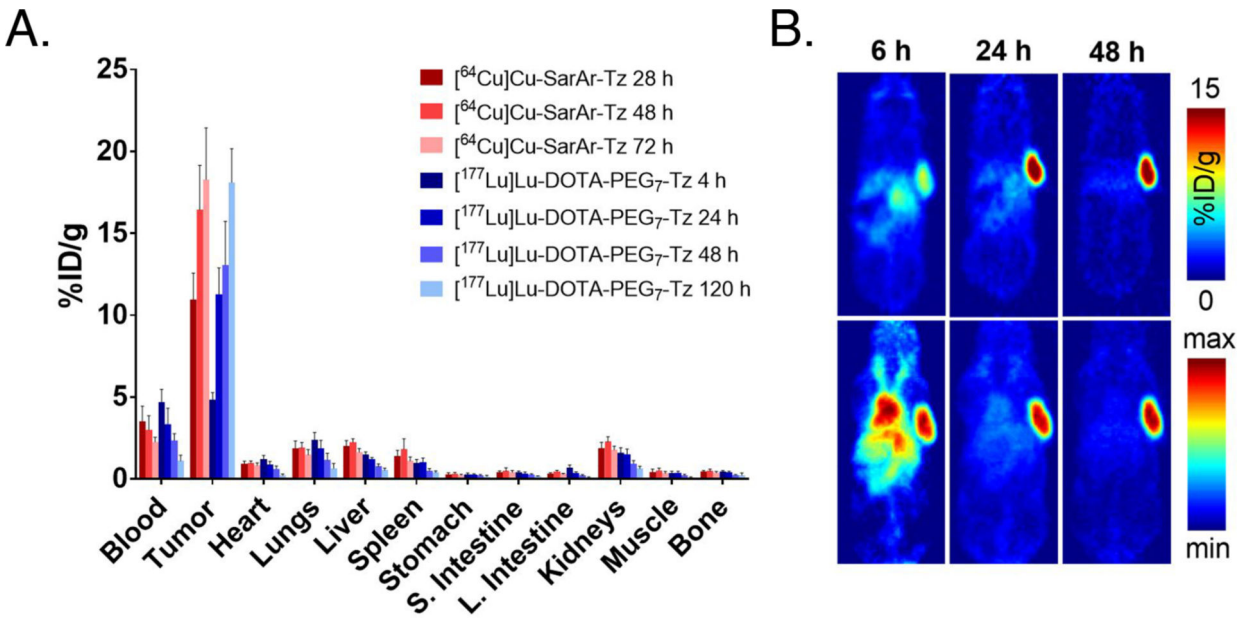

Figure 3.

(A) Biodistribution data for *in vivo* pretargeting (n = 5) using two different tetrazine radiotracers — [^{64}Cu]Cu-SarAr-Tz and [^{177}Lu]Lu-DOTA-PEG$_7$-Tz — in athymic nude mice bearing subcutaneous SW1222 xenografts. The mice were first administered huA33-TCO (100 μg, 0.67 nmol, 2.4 TCO/mAb) via tail vein, followed 24 hours later by the *i.v.* administration of [^{64}Cu]Cu-SarAr-Tz (10.4–11.3 MBq, 0.64–0.69 nmol) and 24 h thereafter by the *i.v.* injection of [^{177}Lu]Lu-DOTA-PEG$_7$-Tz (5.9–6.4 MBq, 0.68–0.73 nmol). The time values represent the number of hours after the administration of each Tz radioligand; (B) PET images of the same mice at 6, 24, and 48 h after the injection of [^{64}Cu]Cu-SarAr-Tz (11.2 MBq, 0.68 nmol). Top row: Coronal planar images that intersect the center of the tumors. Bottom row: maximum intensity projections (MIP).

Table 1.

Biodistribution data for *in vivo* pretargeting (n = 5) using two different tetrazine radiotracers — [^{64}Cu]Cu-SarAr-Tz and [^{177}Lu]Lu-DOTA-PEG$_7$-Tz — in athymic nude mice bearing subcutaneous SW1222 xenografts. The mice were first administered huA33-TCO (100 μg, 0.67 nmol, 2.4 TCO/mAb) via tail vein, followed 24 hours later by the *i.v.* administration of [^{64}Cu]Cu-SarAr-Tz (10.4–11.3 MBq, 0.64–0.69 nmol) and 24 h thereafter by the *i.v.* injection of [^{177}Lu]Lu-DOTA-PEG$_7$-Tz (5.9–6.4 MBq, 0.69–0.74 nmol). The time values represent the number of hours following the administration of each Tz radiotracer (*i.e.* the 28 h column under [^{64}Cu]Cu-SarAr-Tz denotes 28 h after the injection of [^{64}Cu]Cu-SarAr-Tz, whereas the 4 h column under [^{177}Lu]Lu-DOTA-PEG$_7$-Tz denotes 4 h after the injection of [^{177}Lu]Lu-DOTA-PEG$_7$-Tz). The values for the stomach and small intestines include contents.

	[^{64}Cu]Cu-SarAr-Tz			[^{177}Lu]Lu-DOTA-PEG$_7$-Tz			
	28 h	**48 h**	**72 h**	**4 h**	**24 h**	**48 h**	**120 h**
Blood	3.5 ± 0.9	3.0 ± 9	2.3 ± 0.3	4.7 ± 0.8	3.4 ± 1.0	2.4 ± 0.4	1.1 ± 0.4
Tumor	11.0 ± 1.6	16.4 ± 2.7	18.3 ± 3.2	4.9 ± 0.4	11.3 ± 1.6	13.1 ± 2.7	18.1 ± 2.1
Heart	0.9 ± 0.2	1.0 ± 0.1	0.8 ± 0.2	1.2 ± 0.2	0.9 ± 0.2	0.6 ± 0.2	0.2 ± 0.1
Lungs	1.9 ± 0.5	1.9 ± 0.3	1.5 ± 0.3	2.4 ± 0.4	1.9 ± 0.5	1.2 ± 0.4	0.7 ± 0.3
Liver	2.0 ± 0.3	2.3 ± 0.2	1.6 ± 0.2	1.45 ± 0.2	1.2 ± 0.1	0.8 ± 0.2	0.5 ± 0.1
Spleen	1.4 ± 0.3	1.8 ± 0.6	1.1 ± 0.3	1.0 ± 0.2	1.0 ± 0.3	0.5 ± 0.1	0.4 ± 0.1
Stomach	0.3 ± 0.1	0.3 ± 0.1	0.2 ± 0.1	0.3 ± 0.1	0.3 ± 0.1	0.2 ± 0.1	0.2 ± 0.1
S. Intestine	0.4 ± 0.1	0.5 ± 0.2	0.4 ± 0.1	0.4 ± 0.1	0.3 ± 0.1	0.3 ± 0.1	0.2 ± 0.0[3]
L. Intestine	0.3 ± 0.0[4]	0.5 ± 0.1	0.3 ± 0.1	0.7 ± 0.2	0.4 ± 0.1	0.2 ± 0.1	0.1 ± 0.0[3]
Kidneys	1.9 ± 0.4	2.3 ± 0.3	1.8 ± 0.2	1.6 ± 0.3	1.5 ± 0.3	0.9 ± 0.2	0.6 ± 0.2
Muscle	0.4 ± 0.2	0.5 ± 0.1	0.4 ± 0.1	0.4 ± 0.1	0.4 ± 0.1	0.2 ± 0.1	0.1 ± 0.0[3]
Bone	0.5 ± 0.1	0.5 ± 0.1	0.4 ± 0.1	0.5 ± 0.1	0.4 ± 0.1	0.2 ± 0.0[4]	0.2 ± 0.1

Table 2.

Radiation dose rates and therapeutic indices for [^{177}Lu]Lu-DOTA-PEG$_7$-Tz calculated based on the biodistribution data from the huA33-TCO/[^{64}Cu]Cu-SarAr-Tz/[^{177}Lu]Lu-DOTA-PEG$_7$-Tz pretargeting experiment.

Organ	Dose (cGy/MBq)	Therapeutic Index
Tumor	310.2	_
Blood	25.0	12.4
Heart	5.7	54.9
Lungs	11.7	26.5
Liver	11.7	26.5
Spleen	7.2	43.0
Stomach	2.4	131.2
S. Intestine	3.5	87.7
L. Intestine	2.5	124.7
Kidneys	10.6	29.3
Muscle	2.3	134.1
Bone	4.8	65.3